

Calibrations of α Cen A & B

P. Morel¹, J. Provost¹, Y. Lebreton², F. Thévenin¹ and G. Berthomieu¹

¹ Département Cassini, UMR CNRS 6529, Observatoire de la Côte d'Azur, BP 4229, 06304 Nice CEDEX 4, France

² DASGAL, UMR CNRS 8633, Observatoire de Paris-Meudon, 92195 Meudon Principal CEDEX, France.

Received date / Accepted date

Abstract. Detailed evolutionary models of the visual binary α Centauri, including pre main-sequence evolution, have been performed using the masses recently determined by Pourbaix et al. (1999). Models have been constructed using the CEFF equation of state, OPAL opacities, NACRE thermonuclear reaction rates and microscopic diffusion. A χ^2 -minimization is performed to derive the most reliable set of modeling parameters $\wp = \{t_{\alpha \text{ Cen}}, Y_i, [\frac{\text{Fe}}{\text{H}}]_i, \alpha_A, \alpha_B\}$, where $t_{\alpha \text{ Cen}}$ is the age of the system, Y_i the initial helium content, $[\frac{\text{Fe}}{\text{H}}]_i$ the initial metallicity and, α_A and α_B the convection parameters of the two components. Using the basic Böhm-Vitense (1958) mixing-length theory of convection, we derive $\wp_{\text{BV}} = \{2710 \text{ Myr}, 0.284, 0.257, 1.53, 1.57\}$. We obtain a noticeably smaller age than estimated previously, in agreement with Pourbaix et al. (1999), mainly because of the larger masses. If convective core overshoot is considered we get $\wp_{\text{ov}} = \{3530 \text{ Myr}, 0.279, 0.264, 1.64, 1.66\}$. The use of Canuto & Mazitelli (1991, 1992) convection theory leads to the set $\wp_{\text{CM}} = \{4086 \text{ Myr}, 0.271, 0.264, 0.964, 0.986\}$. Using the observational constraints adopted by Guenther & Demarque (2000), and the basic mixing-length theory, we obtain $\wp_{\text{GD}} = \{5640 \text{ Myr}, 0.300, 0.296, 1.86, 1.97\}$ and surface lithium depletions close to their observed values.

A seismological analysis of our calibrated models has been performed. The determination of large and small spacings between the frequencies of acoustic oscillations from seismic observations would help to discriminate between the models of α Cen computed with different masses and to confirm or rules out the new determination of masses.

Key words: Physical data and processes: Convection - Physical data and processes: Diffusion - Stars: binaries: visual - Stars: evolution - Stars: fundamental parameters - Stars: individual: α Cen

1. Introduction

As the Sun's nearest stellar neighbors, the two members of the visual binary α Centauri A & B (G2V + K1V) provide the most accurate potentiality of testing stellar physics in conditions slightly different from the solar ones and then deserve undivided attention for internal structure modeling and oscillation frequencies calculations. By coincidence, the masses and the spectral types of components A/B (HD 128620/1, IDS 14328-6025 A/B, Hipparcos 71 683/1) bracket those of the Sun. The high apparent brightness and the large parallax imply that surface abundances and astrometric parameters are known better than for any star (except the Sun). The basic intent of this paper is to model α Cen A & B using updated physics. This allows to predict of the p -mode oscillation frequencies, which will be useful to exploit future asteroseismological observations as expected, for instance, from the project Concordiaastro at the South Pole (Fossat et al. 2000). Also, as “solar like stars”, the two components are primary targets for the MONS (Kjeldsen et al. 1999b) spatial mission and their oscillations are expected to be well separated in the frequency spectrum.

Based on the reasonable hypothesis of a common origin for both components, i.e. same initial chemical composition and age, the calibration of a binary system consists in determining a consistent evolutionary history for the double star, given (1) the positions of the two components in a H-R diagram, (2) the stellar masses and, (3) the present day surface chemical composition. The goal is to compute evolutionary models that reproduce the observations. This procedure yields estimates for the age t_* , the initial helium mass fraction Y_i and initial metallicity $[\frac{\text{Fe}}{\text{H}}]_i$ (logarithm of the number abundances of iron to hydrogen relative to the solar value), which are fundamental quantities for our understanding of the galactic chemical evolution. We also derive values of the “mixing-length parameter” or “convection parameter” α , ratio of the mixing-length to the pressure scale height. Once the initial masses and the physics are fixed, the modeling of

the two components A & B of a binary system requires a set \wp of five so-called modeling parameters:

$$\wp = \left\{ t_{\star}, Y_i, \left[\frac{\text{Fe}}{\text{H}} \right]_i, \alpha_A, \alpha_B \right\}.$$

In most cases there are only four reliable observables namely, the effective temperatures $T_{\text{eff A}}, T_{\text{eff B}}$ and the luminosities L_A, L_B or the gravity $\log g_A, \log g_B$ of each component. Therefore, one of the unknowns has to be fixed. Very often the mixing-length parameters are assumed to be the same for both components, even if the mass ratio differs significantly from unity. Once detailed spectroscopic analyses have been performed on the system, the precise present day surface metallicities of stars come as additional observational constraints.

In this paper we attempt to reproduce the observed metallicities and, if possible, the lithium depletion by means of models including microscopic diffusion. We calibrate the binary system using both Böhm-Vitense’s (1958, hereafter MLT_{BV}) and Canuto & Mazitelli (1991, 1992, hereafter MLT_{CM}) mixing-length convection theories.

The paper is divided as follows: in Sect. 2, we recall the main results obtained in previous theoretical works and, in Sect. 3, we emphasize the difficulties related to the choice of mixing-length parameters. In Sect. 4, we discuss the modeling of the transport processes acting beneath the convection zone. The observational material, relevant to the evolutionary status of α Cen and available in the literature, is collected in Sect. 5. The method of calibration is described in Sect. 6. In Sect. 7, we present the stellar modeling procedure. In Sect. 8, we give the results with emphasis on the seismological analysis. We summarize our results and conclude in Sect. 9.

2. Previous theoretical works

On the basis of rotational velocity measurements, observed Li abundances and CaII emission intensity, Boesgaard & Hagen (1974) attributed to the system an age of $t_{\alpha \text{ Cen}} = 3.6$ Gyr. Then, several groups calculated stellar evolution models to calibrate the system and draw information on the two components as well as on the physics governing their structure. Table 1 gives the values of the calibration parameters derived in all those studies which we now briefly summarize.

Initially, Flannery & Ayres (1978) and Demarque et al. (1986) could only use the luminosities of α Cen A & B as observational constraints. Flannery & Ayres models support the fact that the system is metal rich with respect to the Sun with $Z_{\alpha \text{ Cen}} \sim 2Z_{\odot}$. Demarque et al. (1986) derived the age of the system as a function of metallicity; they also computed the p -mode oscillation spectrum of α Cen A. Noels et al. (1991) introduced a general procedure for fitting models to the binary system. They derived the age, the helium content and the metallicity of the system and the value of the MLT_{BV} parameter assuming that

it is the same for the two stars. Neuforge (1993) revisited that work using OPAL opacities (Iglesias et al. 1992) complemented by her own low-temperature opacities. Fernandes & Neuforge (1995) showed that the mixing-length parameter α obtained through calibration is different for the two stars and that their values become very similar if the mass fraction of heavy elements increases above $Z \sim 0.035$. They also performed model calibrations with the MLT_{CM} convection treatment with a mixing-length equal to the distance to the top of the convective envelope, thus avoiding the calibration of a convection parameter. In parallel, Edmonds et al. (1992) were the first to add the observed metallicity as a constraint (releasing in turn the hypothesis that α is unique) and to include the effect of microscopic diffusion. More recently, Pourbaix et al. (1999) revisited the calibration of the α Cen system. They calculated a new visual orbit on the basis of available separations, position angles and precise radial velocities measurements and derive new consistent values of the orbital parallax, sum of masses, mass ratio and individual masses. The main result is that the masses of the components are 5% higher and that the helium abundance and age are significantly smaller than previous estimates. Guenther & Demarque (2000) performed several calibrations of the system using different values of the parallax including the Hipparcos value and models calculated with updated physics including helium and heavy elements diffusion. They estimated the uncertainties on the calibrated parameters resulting from the error bars on mass, luminosity, effective temperature and chemical composition.

The differences between these calibrations reflect the great improvements in the description of the stellar microphysics achieved during the last two decades and the progress of the analysis of the observational data. However, uncertainties remain on the transport processes (e.g. convection, microscopic and turbulent diffusion). Apparently none of the previous calibrations has attempted to reproduce the observed surface metallicities (except Guenther & Demarque 2000) and lithium abundances which are fundamental data for the understanding of the transport processes beneath the convection zone of solar-like stars.

As asteroseismology will in a near future strongly constrain the stellar models, some of the above described theoretical works give the main characteristics of the oscillation spectrum of the components ($\Delta\nu_0$ and $\overline{\delta\nu_{02}}$ – see definitions Sect. 8.3.1). The “mean” large separation $\Delta\nu_0$ between the frequencies of modes of a given degree and of consecutive radial order depends on the stellar radius and mass. The “mean” small separation $\overline{\delta\nu_{02}}$ between the frequencies of modes with degree $\ell = 0$ and 2 and consecutive radial order, measured by $\overline{\delta\nu_{02}}$, is sensitive to the structure of the stellar core. Table 1 gives estimates of these quantities from the literature and from this work.

Table 1. Modeling parameters and main characteristics of the oscillation spectrum of α Cen A & B derived in this paper and taken from the literature. The symbols have their usual meaning (see text). The references are: (1) this paper, models A_{BV} & B_{BV}, (2) this paper, models A_{ov} & B_{ov}, (3) this paper, models A_{CM} & B_{CM}, (4) this paper, models A_{GD} & B_{GD}, (5) Flannery & Ayres (1978), (6) Demarque et al. (1986), (7) Noels et al. (1991), (8) Edmonds et al. (1992), (9) Neuforge (1993), (10) Lydon et al. (1993), (11) Pourbaix et al. (1999), (12) Guenther & Demarque (2000).

α_A	α_B	Y_i	$[\frac{\text{Fe}}{\text{H}}]_i$	$(\frac{Z}{X})_i$	$t_{\alpha \text{ Cen}}$ Myr	$\Delta\nu_0^A$ $\mu\text{ Hz}$	$\overline{\delta\nu_{02}^A}$ $\mu\text{ Hz}$	$\Delta\nu_0^B$ $\mu\text{ Hz}$	$\overline{\delta\nu_{02}^B}$ $\mu\text{ Hz}$	
$1.53^{+0.06}_{-0.06}$	$1.57^{+0.03}_{-0.11}$	$0.284^{+0.002}_{-0.002}$	$0.257^{+0.002}_{-0.002}$	0.0443	2710^{+550}_{-690}	108	8.9	154	12.5	(1)
$1.64^{+0.06}_{-0.04}$	$1.66^{+0.04}_{-0.01}$	$0.279^{+0.002}_{-0.002}$	$0.264^{+0.002}_{-0.002}$	0.0450	3530^{+550}_{-690}	107	9.1	154	12.5	(2)
$0.96^{+0.02}_{-0.02}$	$0.99^{+0.06}_{-0.09}$	$0.271^{+0.002}_{-0.004}$	$0.264^{+0.004}_{-0.004}$	0.0450	4090^{+410}_{-690}	108	7.5	157	11.7	(3)
$1.86^{+0.09}_{-0.06}$	$1.97^{+0.13}_{-0.15}$	$0.300^{+0.002}_{-0.002}$	$0.296^{+0.003}_{-0.002}$	0.0480	5640^{+210}_{-210}	102	4.5	161	10.6	(4)
1.33	1.33	0.246		0.04	6000 ± 1000					(5)
1.37	1.37	0.236		0.02-0.04	$3500 - 5500$	118				(6)
1.6	1.6	0.32		0.04	5000 ± 500					(7)
1.15	1.25	0.300 ± 0.005		0.026 ± 0.003	4600 ± 400	108	6.2	179	12.6	(8)
2.10	2.10	0.321		0.038	4840					(9)
1.70 ± 0.1	2.1 ± 0.1	0.298 ± 0.006		0.031 ± 0.002	5600 ± 500					(10)
1.86 ± 0.8	2.1 ± 0.8	0.284 ± 0.058		0.030	2700	107	9			(11)
2.33	2.54	0.280		0.034	7600 ± 800	101	4.6	173	15	(12)

3. The puzzle of the mixing-length parameter

The calibration of a solar model provides the value of the solar mixing-length parameter α_{\odot} which in turn is currently used to model other stars with the same input physics. The value of α_{\odot} changed in time because of successive updates of the input physics, in particular the low-temperatures opacities and model atmospheres. Apart from the difficulty of evaluating α_{\odot} , the question arises whether stars of different masses, initial chemical composition and evolutionary status can be modeled with a unique α . Because models are also used to calculate isochrones, it is important to try to clarify the situation: if α is proved to vary significantly with mass, metallicity and with evolution, the isochrones might have quite different shapes which could modify the age estimates. On the other hand, models of various masses, all computed with α_{\odot} , can reproduce quite well the slope of the main-sequence of the Hyades cluster (Perryman et al. 1998) and of field stars (Lebreton et al. 1999) observed by Hipparcos, indicating that α does not vary much for masses close to the solar mass.

For binaries with well-known properties as α Cen, the question of the universality of the mixing-length parameter has been examined many times. Table 1 shows that among the attempts of calibrating α Cen A & B in luminosities and radii using models based on the MLT_{BV}, two

yield values of α different for each component and different from α_{\odot} (Lydon et al. 1993, Pourbaix et al. 1999) while other calibrations suggest similar values for the two stars (Edmonds et al. 1992, Fernandes & Neuforge 1995). Also, Fernandes et al. (1998) calibrated three other binary systems and the Sun with the same input physics and concluded that α is almost constant for $[\frac{\text{Fe}}{\text{H}}]$ in the range $[\frac{\text{Fe}}{\text{H}}]_{\odot} \pm 0.3$ dex and masses in the range $0.6 - 1.3 M_{\odot}$ while Morel et al. (2000b) found a small difference of α (≈ 0.2) in the two components of the ι Peg system.

As pointed out by many authors (e.g. Lydon et al. 1993, Andersen 1991) accurate masses and effective temperatures are required to draw firm conclusions on whether the MLT_{BV} parameters are different or not. This is also illustrated by the large error bars on α (≈ 0.8) quoted by Pourbaix et al. (1999) which include all possible observable sources of errors including the errors in the masses. For a detailed estimate of the error budget see e.g. Guenther & Demarque (2000).

Some 2-D and 3-D numerical simulations of convection have been performed and translated into effective mixing length parameter (Abbet et al. 1997, Ludwig et al. 1999, Freytag et al. 1999). They suggest that, for stars with effective temperature, gravity and metallicity close to solar the mixing-length parameter remains almost constant. Similar results are obtained by Lydon et al. (1993) who compared models of α Cen A & B based on the results of

numerical simulations of convection and found that a single value of α may be applicable to main sequence solar type stars. In the MLT_{CM} convection theory, Canuto & Mazitelli (1991, 1992) used two modern theories of turbulence to establish a formula for the turbulent convective flux which replaces the MLT_{BV} expression (because the full spectrum of convective eddies is taken into account, the convective efficiency is magnified by about one order of magnitude). The MLT_{CM} theory also makes use of a mixing length which is equal, either to the distance towards the outermost limit of the convection zone, or to the fraction (α) of the pressure scale height. The solar calibration with the MLT_{CM} treatment yields an α_{\odot} value of the order of unity. It is to be noted that for the Sun, models calibrated with MLT_{CM} have frequencies which are closer to the observations than those calibrated with MLT_{BV} (Christensen-Dalsgaard et al. 1996).

4. Diffusion and transport processes

For the Sun, it is now well established that microscopic diffusion by gravitational settling has a measurable impact on models thus on their pulsation spectrum. As time goes on, all chemical species sink in the gravitational well, except the lightest one, ^1H . At the surface, the amount of hydrogen is enhanced while helium and heavy elements are depleted. This implies a decrease of the surface metallicity $[\frac{\text{Fe}}{\text{H}}]_{\text{s}}$ with respect to time. Since the time-scale of abundance variations in the convection zone is roughly proportional to the square root of the mass of the convection zone (Michaud 1977), the microscopic diffusion time-scale decreases with increasing stellar mass implying that diffusion is more efficient in massive stars. As a consequence, a smaller surface metallicity is expected for α Cen A than for α Cen B. This is an additional constraint for the models.

As lithium burns at temperatures close to 3 MK, the observed surface abundance $[\text{Li}]_{\text{s}}$ ($\text{H} \equiv 12$) is often used as a probe for theories of transport processes at work beneath the external convective zone. The microscopic diffusion alone is not efficient enough to explain the lithium depletion observed in the Sun and stars; thus, there is a need for an unknown physical process, e.g. a turbulent mixing, acting in the radiative zone just beneath the outer convection zone – e.g. Schatzman (1996), Montalbán & Schatzman (2000) for a review. According to the present state of the art, either the shear resulting from the different rotational status between the convection zone and the radiative interior (e.g. Zahn 1992), or internal waves (e.g. Montalbán & Schatzman 2000), are believed to be responsible for that turbulence. For stars more massive than the Sun, turbulent mixing is required, in some (hypothetical) mixed stellar mass fraction, to connect and to extend somehow the mixing of the external convection zones. This avoids the complete segregation of helium and heavy elements from the surface and can explain the

AmFm phenomenon (e.g. Richer et al. 2000). Despite numerous attempts, there is today no fully satisfactory prescription for turbulent diffusion able to account for the observed solar lithium depletion; for other stars the situation is even worse! Further information on the mixing processes at work below the outer convection zones can be provided by simultaneous observations of lithium and beryllium, this latter being depleted deeper in the stars at temperatures slightly larger than for lithium.

5. Observations of the visual binary α Cen

The calibration of a binary system is based on the adjustment of the stellar modeling parameters, so that the model of each component at time $t_{\alpha\text{Cen}}$ reproduces the available observables within their error bars. Among different possibilities, one has to choose the most suited set of variables to be used in the calibration according to the observational and theoretical material available. As aforementioned, because of the assumption of a common origin of both components, five unknowns enter the modeling of their evolution. There are six most currently available constraints: (1) the effective temperatures for α Cen A & B, derived from precise detailed spectroscopic analysis, (2) either the spectroscopic gravities or the luminosities, these latter derived from the photometric data and parallax, using bolometric corrections (3) the surface metallicities. In the following, we discuss all the relevant available observations and we choose the most appropriate and accurate observables to be fitted in the calibration process.

5.1. Astrometric data

For a visual binary, the parallax uncertainty is the largest source of error in the derivation of the sum of masses via the third Kepler law (Couteau 1978, 40, VI). Unfortunately, α Cen was “difficult” for Hipparcos with the secondary at the edge of the sensitivity profile (Söderhjelm 2000). Söderhjelm improved the adjustment of the Hipparcos parallax by taking into account the known orbital motion but, as expected, the orbital curvature covered during the 3.25 yr mission, was not sufficient to derive a reliable mass ratio of the components. Table 2 shows that the new parallax value differs from the former by more than 2σ . With respect to the original Hipparcos value this new one is closer to the long focus photographic determination of Kamper & Wesselink (1978) based on Heintz’s (1958) orbital elements.

After numerous independent investigations during almost 100 years, Pourbaix et al. (1999) derived an orbit based both on visual astrometric and precise radial velocity data, leading to consistent determinations of orbital parameters, orbital parallax, sum of masses, mass ratio and, thus, precise mass values for α Cen A & B. Here, we prefer to use of Pourbaix et al. (1999) mass values because Söderhjelm’s (2000) ones are based on disparate

Table 2. Astrometric properties of the α Centauri A & B binary system. P is the orbital period in yr, a the semi major axis in arc second, ϖ the parallax in mas, $K = M_B/(M_A + M_B)$ the fractional mass.

P	a	ϖ	K	M_A/M_\odot	M_B/M_\odot	References
79.92	17.515	750	0.453	1.09	0.90	Heintz (1958), (1982)
		749 ± 5	0.454 ± 0.02	1.10	0.91	Kamper & Wesselink (1978)
		750.6 ± 4.6				Demarque et al. (1986)
		742.1 ± 1.4				ESA (1997)
79.90 ± 0.01	17.59 ± 0.03	737.0 ± 2.6	0.45 ± 0.1	1.16 ± 0.03	0.97 ± 0.03	Pourbaix et al. (1999) (orbital parallax)
		747.1 ± 1.2				Söderhjelm (2000)

sources (i.e., Hipparcos parallax, Heintz’s (1958) orbit and the mass ratio of Kamper & Wesselink (1978)). We do not take into account mass errors in the calibrations.

The inclinations of the orbits of Heintz (1958, 1982) and Pourbaix et al. (1999) agree within less than one tenth of a degree, $i = 79^\circ 29 \pm 0^\circ 01$, $\sin i \simeq 1$ (the Sun lies close to the orbital plane of α Cen). With the reasonable assumption that the orbital and rotational axis are parallel, owing to the high inclination, α Cen A & B are seen about equator on and the observed rotational velocities are close to their equatorial values, $v \sin i \simeq v$.

5.2. Photometric data

Photometric data are available in the V , B (Mermilliod et al. 1997) and K (Thomas et al. 1973) bands. But, as claimed by Flannery & Ayres (1978) and Chmielewski et al. (1992), the dynamical range of commonly used photometers is limited, which does not allow precise photometric measurements of bright stars. This makes the α Cen photometric data rather unsafe (Chmielewski et al. 1992) and we preferred to use the spectroscopic data. However, for comparison, we have used these photometric data to derive bolometric corrections and effective temperatures of the two components from (1) the empirical calibrations of Alonso et al. (1995, 1996) and (2) the theoretical calibrations of Lejeune et al. (1998). The $T_{\text{eff}}(V - K, [\frac{\text{Fe}}{\text{H}}])$ empirical calibration of Alonso et al. (1996) leads to $T_{\text{eff,A}} = 5738 \pm 40$ K and $T_{\text{eff,B}} = 5165 \pm 70$ K while the theoretical (based on model atmospheres) calibrations of Lejeune et al. (1998) yield $T_{\text{eff,A}} \simeq 5800$ K and $T_{\text{eff,B}} \simeq 5250$ K, all well compatible with spectroscopic temperatures. The $F_{\text{bol}}(V - K, [\frac{\text{Fe}}{\text{H}}])$ empirical calibration of the bolometric flux (Alonso et al. 1995) provides bolometric corrections $\text{BC}_A(V) = -0.09$ and $\text{BC}_B(V) = -0.23$ close to the values inferred from the theoretical calibrations of Lejeune et al. (1998) (-0.11 and -0.23 respectively). Let us point out that these bolometric corrections are larger than those adopted by Guenther & Demarque (2000).

Table 4. Atmospheric abundances of α Cen A & B. The references are: (1) Furenlid & Meylan (1990), (2) Neuforge-Verheecke & Magain (1997), (3) Thévenin (1998).

	α Cen A		α Cen B	
C	0.20 (2)	0.14 (1)		0.28 (2)
N		0.30 (2)		
O	0.15 (3)	0.21 (2)	0.10 (1)	
Al	0.30 (3)	0.24 (2)	0.23 (1)	0.40 (3) 0.24 (2)
Si	0.35 (3)	0.27 (2)	0.20 (1)	0.45 (3) 0.27 (2)
Ca	0.30 (3)	0.22 (2)	0.13 (1)	
Sc	0.30 (3)	0.25 (2)	0.13 (1)	0.26 (2)
Ti	0.25 (3)	0.25 (2)	0.08 (1)	0.27 (2)
V	0.30 (3)	0.23 (2)	0.08 (1)	0.32 (2)
Cr	0.25 (3)	0.25 (2)	0.13 (1)	0.27 (2)
Mn		0.23 (2)	0.25 (1)	0.26 (2)
Fe	0.20 (3)	0.25 (2)	0.12 (1)	0.22 (3) 0.24 (2)
Co	0.35 (3)	0.28 (2)	0.16 (1)	0.26 (2)
Ni	0.28 (3)	0.30 (2)	0.16 (1)	0.30 (2)
Y	0.20 (3)	0.20 (2)	0.05 (1)	0.14 (2)
Zr	0.20 (3)	0.17 (2)	0.04 (1)	
La	0.40 (3)			
Ce	0.40 (3)			
Nd	0.35 (3)	0.20 (2)		
Sm	0.40 (3)			
Eu		0.15 (2)		

5.3. Spectroscopic data and atmospheric parameters

For both stars many spectroscopic data exist in the literature with good signal to noise ratios because of their high magnitudes. As Table 3 exhibits rather scattered results we decided to reestimate the effective temperatures, surface gravities and metallicities. For our analysis we used the spectroscopic data published by Chmielewski et al. (1992) and Neuforge-Verheecke & Magain (1997), the atmosphere models of Bell et al. (1976) grid and the basic technique of the curve of growth.

Table 3. Spectroscopic data of the α Cen system. The effective temperatures are in K, the metallicities and the lithium abundance in dex. For sake of brevity the uncertainties are not recalled.

$T_{\text{eff A}}$	$T_{\text{eff B}}$	$\log g_A$	$\log g_B$	$[\frac{\text{Fe}}{\text{H}}]_A$	$[\frac{\text{Fe}}{\text{H}}]_B$	$[\text{Li}]_A$	$[\text{Li}]_B$	References
5793	5362			0.22	0.12			French & Powell (1971)
5727	5250	4.38	4.73	0.29	0.37			England (1973)
5820	5350			-0.01	-0.05			Bessell (1981)
						1.28		Soberblom & Dravins (1984)
5720		4.27		0.15				Rabolo et al. (1986)
5793	5305	4.40	4.65	0.20	0.20			Smith et al. (1986)
5793	5305	4.50	4.50	0.20	0.14			Abia et al. (1988)
5727	5250	4.42	4.65	0.20	0.26			Edvardsson (1988)
5727		4.27		0.10				Furenlid & Meylan (1990)
5800	5325	4.31	4.58	0.22	0.26	1.3	≤ 0.4	Chmielewski et al. (1992)
5720		4.27		0.15				Edvardsson et al. (1993)
5830	5255	4.34	4.51	0.25	0.24			Neuforge-Verheeecke & Magain (1997)
						1.37		King et al. (1997)
5730	5250	4.2	4.6	0.20	0.22			Thévenin (1998)
5790	5260	4.32	4.51	0.20	0.23			This paper

5.3.1. Effective temperatures

Table 3 presents effective temperatures compiled from the literature. Chmielewski et al. (1992) derived the effective temperatures from the best fit of the wings of the H_α line. Recently Neuforge-Verheeecke & Magain (1997) obtained the T_{eff} by forcing the abundances derived from FeI lines to be independent of their excitation potential. They not only used the FeI lines to determine the effective temperature of each star but also checked their results using the H_α line profiles. In α Cen A, the two methods lead to consistent results that are also in good agreement with those of Chmielewski et al. (1992), although the two analyses made use of different model atmospheres. In α Cen B, the two methods lead to marginally discrepant results possibly due to Non-LTE effects and to the sensitivity of H_α to the treatment of convection.

We have reconsidered the fit of hydrogen lines of Chmielewski et al. (1992). We took into account the overabundance of the α Cen system which strengthens the metallic lines and displaces the pure wings of H lines; we also took into account the relative strength of metallic lines in α Cen B, different from what is found in solar-like profiles, because of the lower temperature. Consequently, the fit proposed by Chmielewski et al. (1992) seems to overestimate the temperature and we displace it toward cooler values, more importantly in the case of α Cen B. Our adopted effective temperatures are respectively 5790 ± 30 K and 5260 ± 50 K for α Cen A & B. These new proposed temperatures agree, within the 1σ error bars, with the FeI based temperature determinations of

Neuforge-Verheeecke and Magain (1997) and, as quoted in Sect. 5.2, they are close to the values based on Lejeune et al. (1998) calibrations.

5.3.2. Surface gravities

Usually $\log g$, the logarithm of the surface gravity, is determined by the detailed spectroscopic analysis using the ionization equilibrium of iron. Table 3 shows the results obtained by different authors. We remind that the surface gravities from Neuforge-Verheeecke & Magain (1997) and from Chmielewski et al. (1992) are very close. Using the published equivalent width (hereafter EW) and the error bars of Neuforge-Verheeecke & Magain, we derive by the basic curve of growth procedure $\log g_A = 4.32 \pm 0.05$ and $\log g_B = 4.51 \pm 0.08$ for α Cen A & B, respectively.

5.3.3. Chemical composition

Furenlid & Meylan (1990) and Neuforge-Verheeecke & Magain (1997) have found an average metal overabundance of around 0.2 dex. As in Sect. 5.3.2, using oscillator strengths, microturbulence parameter, EW, published by Neuforge-Verheeecke & Magain and the iron curve of growth derived as aforesaid, we get $[\frac{\text{Fe}}{\text{H}}]_A = 0.20 \pm 0.02$ dex and $[\frac{\text{Fe}}{\text{H}}]_B = 0.23 \pm 0.03$ dex for α Cen A & B, respectively; the error bars are from Neuforge-Verheeecke & Magain. We note that metallicities agree, within the 1σ error bars, with the values of Neuforge-Verheeecke & Magain.

Table 4 shows that C, N, O and Fe, the most abundant “metals” and electron donors, have uniform over-

abundances of about ~ 0.2 dex. In consequence, it is reasonable to construct models having a uniform abundance of all metals enhanced by a factor 1.7, corresponding to 0.2 dex compared to the Sun, and use opacities with solar mixture. On the main-sequence, for stellar masses close to the solar one, the differential segregation between the metals does not significantly modify the models (Turcotte et al. 1998) this permits, for the equation of state and opacity data, to keep the ratios between “metals” to their initial value despite the differential segregation by microscopic diffusion and gravitational settling.

Table 3 reveals a good agreement between the measurements of the lithium abundance. α Cen A presents a depletion close to the solar one ($[\text{Li}]_{s\odot} = 1.11$, Grevesse & Sauval 1998) while, in α Cen B, the lithium is clearly more depleted. The assumption of a common origin of the two stars eliminates the possibility of a different initial lithium abundance in the pre-stellar nebulae. Neither an error on temperatures nor on surface gravities in model atmospheres can explain these differences with the solar depletion.

The situation is similar for ^9Be . Observations by Primas et al. (1997) indicate that ^9Be is depleted in α Cen B while α Cen A exhibits a quasi-solar abundance.

5.3.4. Rotation

For α Cen A, Boesgaard & Hagen (1974) estimated a rotational period 10% larger than the solar one. More recently Saar & Osten (1997) measured rotational velocities for α Cen A & B of respectively $2.7 \pm 0.7 \text{ km s}^{-1}$ and $1.1 \pm 0.8 \text{ km s}^{-1}$, in good agreement with other determinations. With the estimated radius of $R_{\alpha \text{ Cen A}} \simeq 1.2R_{\odot}$ and $R_{\alpha \text{ Cen B}} \simeq 0.91R_{\odot}$, the periods of rotation are respectively $P_{\alpha \text{ Cen A}} \simeq 22$ d, and $P_{\alpha \text{ Cen B}} \simeq 41$ d. They bracket the solar value.

5.4. Seismological observations

Many attempts have been made to detect solar-like p -mode oscillations in α Cen A, from ground-based observations. They lead to controversial results. Gelly et al. (1986) reported a detection, but the claimed mean large separation between the oscillation frequencies $\Delta\nu_0 = 165.5 \mu\text{Hz}$ was very large and inconsistent with the theoretical value (Demarque et al. 1986). Despite the use of more sensitive techniques, Brown & Gilliland (1990) failed to detect any oscillation and gave an upper limit for the amplitude of 0.7 ms^{-1} , i.e. 2-3 times the solar one. Pottasch et al. (1992) have detected oscillations in α Cen A. They found a set of regularly spaced peaks, with a mean separation corresponding to $\Delta\nu_0 = 110 \mu\text{Hz}$, consistent with the known properties of this star, but with an amplitude of oscillation larger than the upper limit of Brown & Gilliland (1990). Edmonds & Cram (1995) did not detect unambiguously the p -mode oscillations, but they

found an evidence for almost the same periodicity as that found by Pottasch et al. (1992) in the power spectrum. More recently, Kjeldsen et al. (1999a) found tentative evidence for p -mode oscillations in α Cen A, from equivalent width measurements of the Balmer hydrogen lines. They proposed four different possible identifications of the eight observed frequency peaks in the power spectrum, which correspond to sets of the large and small frequency spacings $\Delta\nu_0$ and $\overline{\delta\nu}_{0,2}$ of (106.94, 12.30), (106.99, 8.15), (100.77, 11.70) and (100.77, 6.42), in μHz . The frequency resolution of the seismological observations will be much improved in a near future, up to $0.1 \mu\text{Hz}$, with several ground-based and space projects.

5.5. Adopted observables constraining the models

To constrain the models at present day, contrarily to previous works, we prefer to use the spectroscopic gravities we derived consistently from effective temperature and metallicities instead of the luminosity derived from the photometry, bolometric correction and parallax. Table 5 gives the effective temperatures, gravities and metallicities we selected to constrain the models. The masses are from Pourbaix et al. (1999). We emphasize that the parallax is required to derive the masses but neither the effective temperatures nor the gravities.

While this work was under investigation, Guenther & Demarque (2000) published new calibrations of the α Cen binary system. As a matter of comparison we have calibrated the α Cen binary system with their constraints. Table 5 presents the observable constraints of the “best” model of Guenther & Demarque (2000). They significantly differ from ours, though correspondingly to almost the same mass ratios. The trigonometrical parallax of Söderhjelm (2000) is larger than the orbital parallax of Pourbaix et al. (1999) and leads to smaller masses and larger (*respt.* smaller) luminosity for α Cen A (*respt.* α Cen B).

6. The method of calibration

The calibration of a binary system is based on the adjustment of stellar modeling parameters to observational data at the age of the system. For a given mass, fixing the physics, the effective temperature, surface gravity and metallicity of a model have the formal dependences with respect to modeling parameters:

$$\begin{aligned} T_{\text{eff}}(\star)_{\text{mod}} &= T_{\text{eff}}\left(t_{\star}; Y_i, \left[\frac{\text{Fe}}{\text{H}}\right]_i, \alpha_{\star}\right), \\ \log g(\star)_{\text{mod}} &= \log g\left(t_{\star}; Y_i, \left[\frac{\text{Fe}}{\text{H}}\right]_i, \alpha_{\star}\right), \\ \left[\frac{\text{Fe}}{\text{H}}\right]_{s}(\star)_{\text{mod}} &= \left[\frac{\text{Fe}}{\text{H}}\right]_{s}\left(t_{\star}; Y_i, \left[\frac{\text{Fe}}{\text{H}}\right]_i, \alpha_{\star}\right). \end{aligned}$$

The basic idea of the χ^2 fitting has been developed by Lastennet et al. (1999). To find a set of modeling parameters:

$$\wp_{\alpha \text{ Cen}} \equiv \left\{ t_{\alpha \text{ Cen}}, Y_i, \left[\frac{\text{Fe}}{\text{H}} \right]_i, \alpha_A, \alpha_B \right\},$$

leading to observables as close as possible to the observations $T_{\text{eff}}(\star)$, $\log g(\star)$ and $\left[\frac{\text{Fe}}{\text{H}} \right]_s(\star)$, we minimize the $\chi^2(t_\star, Y_i, \left[\frac{\text{Fe}}{\text{H}} \right]_i, \alpha_A, \alpha_B)$ functional defined as:

$$\begin{aligned} \chi^2 = & \sum_{\star=A,B} \left(\frac{T_{\text{eff}}(\star)_{\text{mod}} - T_{\text{eff}}(\star)}{\sigma(T_{\text{eff}}(\star))} \right)^2 + \\ & + \left(\frac{\log g(\star)_{\text{mod}} - \log g(\star)}{\sigma(\log g(\star))} \right)^2 + \\ & + \left(\frac{\left[\frac{\text{Fe}}{\text{H}} \right]_s(\star)_{\text{mod}} - \left[\frac{\text{Fe}}{\text{H}} \right]_s(\star)}{\sigma\left(\left[\frac{\text{Fe}}{\text{H}} \right]_s(\star)\right)} \right)^2, \end{aligned} \quad (1)$$

where $\sigma(T_{\text{eff}}(\star))$, $\sigma(\log g(\star))$ and $\sigma\left(\left[\frac{\text{Fe}}{\text{H}} \right]_s(\star)\right)$ are the uncertainties associated to each star. For a grid of modeling parameters \wp , we have computed main-sequence evolution of models with α Cen A & B masses. Then the χ^2 was computed using Eq. (1) in a refined grid obtained by interpolations. We kept for the solution the “best” $\wp = \wp_{\alpha \text{ Cen}}$ which corresponds to the χ^2_{min} . These best modeling parameters are used to compute models of α Cen A & B including pre main-sequence and their frequencies. We do not further attempt neither to improve nor to investigate the stability of the solution via the steepest descent method (Noels et al. 1991, Morel et al. 2000b). Table 1 shows the confidence limits of modeling parameters of models computed in this paper. The confidence limits of each modeling parameter, the other being fixed, correspond to the maximum/minimum values it can reach, in order that the generated models fit the observable targets within their error bars.

7. Evolutionary models

Basically the physics employed for the calculation of models is the same as in Morel et al. (1997). The ordinary assumptions of stellar modeling are made, i.e. spherical symmetry, no rotation, no magnetic field, no mass loss. It has been already claimed, see Morel et al. (2000a), that stellar models of about one solar mass, computed with the same physics but initialized either on pre main-sequence or at zero-age homogeneous main-sequence are almost identical after a few 10^7 years, a small quantity with respect to the expected age of the α Cen system. To save computations, along the search of a solution with the χ^2 minimization, we have initialized each evolution with a homogeneous zero-age main-sequence model. The models presented in Table 5 include the pre main-sequence evolution. They are initialized with homogeneous zero-age stellar model in quasi-static contraction with a central temperature close to the onset of the deuteron burning, i.e. $T_c \sim 0.5$ MK.

7.1. Nuclear and diffusion network.

We have taken into account the most important nuclear reactions of PP+CNO cycles (Clayton, 1968). The relevant nuclear reaction rates are taken from the NACRE compilation (Angulo et al. 1999) with the reaction ${}^7\text{Be}(e^-, \nu\gamma){}^7\text{Li}$ taken from the compilation of Adelberger et al. (1998). Weak screening (Salpeter 1954) is assumed. We have used the meteoritic value (Grevesse & Sauval 1998) for the initial lithium abundance, $[\text{Li}]_i = 3.31 \pm 0.04$. For the calculations of the depletion, lithium is assumed to be in its most abundant isotope ${}^7\text{Li}$ form. The initial abundance of each isotope is derived from isotopic fractions and initial values of $Y \equiv {}^3\text{He} + {}^4\text{He}$ and Z in order to fulfill the basic relationship $X + Y + Z \equiv 1$ with $X \equiv {}^1\text{H} + {}^2\text{H}$. For the models computed for the χ^2 fitting, the isotopes ${}^2\text{H}$, ${}^7\text{Li}$, ${}^7\text{Be}$ are set at equilibrium.

Microscopic diffusion is described by the simplified formalism of Michaud & Proffitt (1993) with heavy elements as trace elements. We have neglected the radiative accelerations as they amount only to a tiny fraction of gravity in the radiative part for stars with masses close to the solar one (Turcotte et al. 1998). We assume that changes of Z , as a whole, describe the changes of metals and we use the approximation:

$$\begin{aligned} \left[\frac{\text{Fe}}{\text{H}} \right] & \equiv \log\left(\frac{Z_{\text{Fe}}}{Z}\right) + \log\left(\frac{Z}{X}\right) - \log\left(\frac{Z_{\text{Fe}}}{X}\right)_{\odot} \simeq \\ & \simeq \log\left(\frac{Z}{X}\right) - \log\left(\frac{Z}{X}\right)_{\odot} \end{aligned}$$

with $\frac{Z_{\text{Fe}}}{Z}$ is the iron mass fraction within Z .

7.2. Equation of state, opacities, convection and atmosphere.

We have used the CEFF equation of state (Christensen-Dalsgaard & Däppen 1992) and the opacities of Iglesias & Rogers (1996) complemented at low temperatures by Alexander & Ferguson (1994) opacities for the solar mixture of Grevesse & Noels (1993). We have not taken into account the changes of abundance ratios between the metals within Z due to diffusion; for stellar masses close to the solar one they do not really affect the structure of models (Turcotte et al. 1998).

In the convection zones the temperature gradient is computed according to either MLT_{BV} or MLT_{CM} convection theories. The mixing-length is defined as $l \equiv \alpha H_p$, where H_p is the pressure scale height. The convection zones are mixed via a strong full mixing turbulent diffusion coefficient $d_m = 10^{13} \text{ cm}^2 \text{ s}^{-1}$ which produces a homogeneous composition (Morel 1997).

At the end of the pre main-sequence both components, have for a few million years, a temporary convective core. For α Cen A, slightly more massive than the Sun, a second convective core is formed during the main-sequence due to the onset of the CNO burning (e.g. Guenther & Demarque 2000). Following the prescriptions of Schaller et

al. (1992) we have calibrated models with overshooting of convective cores over the distance $O_v = 0.2 \min(H_p, R_{co})$ where R_{co} is the core radius.

The atmosphere is restored using a grid of $T(\tau, T_{\text{eff}}, g)$ laws, provided by Cayrel (2000), (τ is the Rosseland optical depth) derived from atmosphere models with the solar mixture of Grevesse & Noels (1993) and metallicity $[\frac{\text{Fe}}{\text{H}}] = 0.2$. The atmosphere models were computed with the Kurucz (1991) ATLAS12 package. The connection with the envelope is made at the optical depth $\tau_b = 20$ where the diffusion approximation for radiative transfer becomes valid (Morel et al. 1994). A smooth connection of the gradients is insured between the uppermost layers of the envelope and the optically thick convective bottom of the atmosphere. It is an important requirement for the calculation of eigenmode frequencies. The radius R_\star of any model is taken at the optical depth τ_\star where $T(\tau_\star) = T_{\text{eff}}$. Typically, τ_\star increases from $\tau_\star \sim 0.43$ in the initial pre main-sequence model, until $\tau_\star \sim 0.53$ at the present time. The mass of the star M_\star is defined as the mass enclosed in the sphere of radius R_\star . The external boundary is located at the optical depth $\tau_{\text{ext}} = 10^{-4}$, where the density is fixed to its value in the atmosphere model $\rho(\tau_{\text{ext}}) = 2.22 \cdot 10^{-9} \text{ g cm}^{-3}$. To simplify, the chemical composition within the atmosphere models is assumed to be unaffected by the diffusion.

7.3. Numerics.

Models have been computed using the CESAM code (Morel 1997). The numerical schemes are fully implicit and their accuracy is of the first order for the time and third order for the space. Each model is described by about 600 mass shells, this number increases up to 2100 for the models used in seismological analysis. Evolutions are described by about 80 models. About half of them concerns the pre main-sequence evolution.

8. Results

For different sets of modeling parameters we have computed evolutionary tracks using the convection theories of Böhm-Vitense (1958, MLT_{BV}) and Canuto & Mazitelli (1991, 1992, MLT_{CM}). Using the χ^2 minimization described in Sect. 6, we have selected the best fits taking into account the accuracy of the observational constraints. Tables 1 and 5 (bottom panel) present the characteristics of α Cen A & B and Sun models computed with the same input physics. Figure 1 presents the evolutionary tracks in the $\log L/L_\odot$ versus $\log T_{\text{eff}}$ H-R diagram. We also performed χ^2 minimization with the constraint $\alpha_A \equiv \alpha_B$, but, for brevity sake, we do not report the results as they do not significantly differ from those obtained without this constraint. For all α Cen A models a convective core, caused by an enhancement of the CNO nuclear energy generation, appears as soon as the central temperature becomes

slightly larger than 17 MK and the mass fraction of hydrogen $X_c \gtrsim 0.37$. Figure 1, Tables 1 and 5 clearly show that various sets of modeling parameters allow to verify the observational constraints within the error bars. In absence of seismological observations there is no criterion available to discriminate between models. Tables 1 and 5 show that, within the confidence domains, the values of the mixing length parameter of the two components are very close.

8.1. MLT_{BV} models.

Models A_{BV} & B_{BV} have an age $t_{\alpha \text{ Cen}} = 2710 \text{ Myr}$ compatible with the estimate of Pourbaix et al. (1999). The values of the convection parameters are almost equal ($\alpha_A \simeq \alpha_B$) and close to the value derived if they are forced to be identical in the χ^2 minimization. They are quite close to the value obtained by Noels et al. (1991) but differ notably from the estimate of Pourbaix et al. (1999) though remaining within their large confidence domains. They are smaller than the solar value α_\odot . In α Cen A a convective core is formed at time $t \sim 2.6 \text{ Gyr}$ a few Myr just before $t_{\alpha \text{ Cen}}$. Figure 1, bottom panels, shows the loci in the H-R diagram reached by the A_{BV} & B_{BV} models when one modeling parameter changes within its uncertainty domain, the other modeling parameters being fixed. The limited extents of the permitted solutions are consequences of limits in metallicity. Table 6 shows the partial derivatives of the observed parameters with respect to the modeling ones. Our results are similar to those of Brown et al. (1994), except for the derivatives with respect to the age which are very dependent on the exact evolutionary stage on the main sequence. As already noticed by Guenther & Demarque (2000), the luminosities are very sensitive to the helium mass fraction (see the large values of their derivatives with respect to Y_i in Table 6), which in turn gives a narrow confidence level for the initial helium abundance (see Table 1).

For both components the surface lithium depletion is not sufficient enough to fit the observed values.

Models A_{ov} & B_{ov} with overshooting of convective cores have an age significantly larger than models A_{BV} & B_{BV} . Indeed their outer convective zones penetrate deeper. For model B_{ov} this depletion is marginally compatible with the observation, while it is not large enough for model A_{ov} . All these differences with models A_{BV} & B_{BV} , of course, result from the overshooting of convective cores but in a roundabout way via the χ^2 minimization which adjusts the modeling parameters as a whole. The convective core of model A_{ov} is formed at time $t \sim 3.16 \text{ Gyr}$.

Models A_{GD} & B_{GD} are calibrated according to the Guenther & Demarque (2000) observational constraints and masses. The age, initial helium mass fraction and metallicity and the convection parameters are significantly

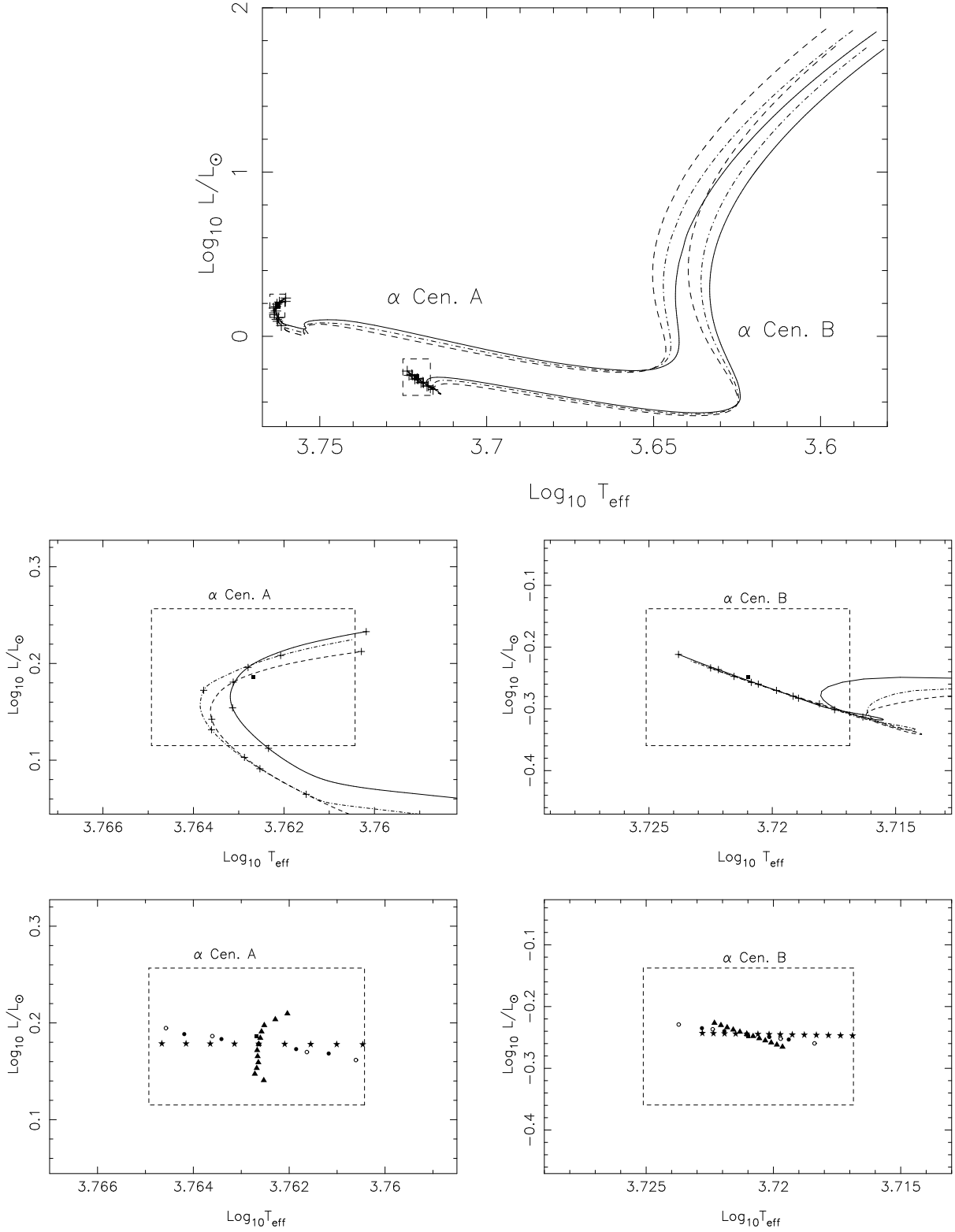


Fig. 1. Evolutionary tracks in the H-R diagram of models A_{BV} , B_{BV} (full), A_{CM} , B_{CM} (dashed) and A_{ov} , B_{ov} (dot-dash-dot). Dashed rectangles delimit the uncertainty domains. Top panel: full tracks from PMS. The stellar evolution sequences are initialized on the pre main-sequence soon after the deuterium ignition. The “+” denote 1 Gyr time intervals along the evolutionary tracks. Middle left and right panels: enlargements around the observed α Cen A, & B loci. Bottom left and right panels: loci of α Cen A & B models computed with the MLT_{BV} convection theory and modeling parameters within the confidence domains presented in Table 5; full triangle: $t_{\alpha Cen}$ changes only, full star: α changes only, empty circle: Y_i changes only and full dot: $[\frac{Fe}{H}]_i$ changes only.

larger than those derived using the mass values of Pourbaix et al. (1999). We have obtained similar modeling parameters from the χ^2 minimization using models with Guenther & Demarque (2000) masses and our observational constraints. Therefore, the differences between the modeling parameters of models A_{BV} & B_{BV} and A_{GD} & B_{GD} mainly result from the mass differences, but also from the disparity of observing targets, although in a less extent. For models A_{GD} & B_{GD} the convection parameters are close to the solar value. In the model A_{GD} the convective core is formed at the time $t \sim 3.7$ Gyr, larger than in other MLT_{BV} models and the lithium depletion at the surface is marginally compatible with the observed value. The value of the central hydrogen mass fraction is half that obtained in the other MLT_{BV} models. In model B_{GD} the lithium depletion is compatible with the observation.

8.2. MLT_{CM} models.

In agreement with Canuto & Mazitelli (1991, 1992) convection theory, the convection parameters of models A_{CM} & B_{CM} are close to unity and close to the solar value. The age is slightly smaller than the solar one but larger than that of models A_{BV} & B_{BV} ; the outer convection zone is deeper. According to the observations, the lithium of model B_{CM} is almost totally depleted but practically no depletion occurred in models A_{CM} and the solar one. The convective core of model A_{CM} is formed at time $t \sim 3.9$ Gyr.

8.3. Seismological analysis of α Cen A & B

The stars α Cen A & B are solar-like stars. The oscillations of such stars may be stochastically excited by the convection as in the case of the Sun. The amplitudes of solar-like oscillations have been estimated for stars of different masses and ages (Houdek 1996, Houdek et al. 1999). The models we have calibrated are close in the H-R diagram, but have different internal structure and they could be discriminated with the help of seismology. The properties of the stellar oscillations are related to the variation along the radius of the sound speed c and of the Brunt-Väissälä frequency N (Christensen-Dalsgaard & Berthomieu 1991). The p -mode frequencies are mainly related to c , while the g -modes, with lower frequencies, are determined essentially by N . We have computed for all our models the adiabatic frequencies of oscillation for modes of low degrees $\ell=0$ to 3, which may be detected by future observations. Table 8 presents the p -mode frequencies for the models A_{BV} and B_{BV} . As in the solar case (Provost et al. 2000), the lowest frequency p -mode oscillations of α Cen A have a mixed character between p - and g -mode behavior and are very sensitive to the structure of the central stellar regions.

Table 7. Theoretical global asymptotic characteristics of the low degree p -mode and g -mode spectrum of the star α Cen A & B. The quantities ν_{00} , $\Delta\nu_0$, $\overline{\delta\nu_{0,2}}$ and $\overline{\delta\nu_{1,3}}$ ($n_0 = 21$), describing the p -mode oscillations, are given in μHz - see definitions Sect. 8.3.1. The characteristic g -mode period P_0 is given in mn. The lower panel presents the variations $\Delta[\Delta\nu_0]$, $\Delta[\overline{\delta\nu_{0,2}}]$, $\Delta[\overline{\delta\nu_{1,3}}]$ and $\Delta[P_0]$ for the models computed with the MLT_{BV} theory and extreme modeling parameters α , $t_{\alpha\text{Cen}}$, Y_i and $[\frac{\text{Fe}}{\text{H}}]_i$ within the confidence domains presented in Table 1.

	ν_{00}	$\Delta\nu_0$	$\overline{\delta\nu_{0,2}}$	$\overline{\delta\nu_{1,3}}$	P_0
A_{BV}	2391.0	108.1	8.9	14.7	44.8
A_{ov}	2365.9	106.8	9.1	13.6	56.3
A_{CM}	2397.3	108.1	7.5	12.8	44.3
A_{GD}	2256.9	101.7	4.4	9.7	49.2
B_{BV}	3456.8	154.0	12.5	20.6	55.5
B_{ov}	3467.2	154.3	12.0	19.8	52.1
B_{CM}	3546.4	157.4	11.7	19.5	50.9
B_{GD}	3603.7	160.2	10.7	18.4	43.6
		$\Delta[\Delta\nu_0]$	$\Delta[\overline{\delta\nu_{0,2}}]$	$\Delta[\overline{\delta\nu_{1,3}}]$	$\Delta[P_0]$
A_{BV}					
$\Delta\alpha_A = 0.12$	2.9	0.1	0.3	0.4	
$\Delta t_{\alpha\text{Cen}}=1300$	-9.7	-1.7	-3.1	3.1	
$\Delta Y_i=0.004$	-0.9	-0.1	-0.3	3.6	
$\Delta[\frac{\text{Fe}}{\text{H}}]_i = 0.004$	0.2	0.01	0.04	0.2	
B_{BV}					
$\Delta\alpha_B = 0.14$	3.6	0.1	0.2	0.2	
$\Delta t_{\alpha\text{Cen}}=1300$	-5.4	-1.2	-1.6	-8.2	
$\Delta Y_i=0.004$	-1.1	-0.1	-0.1	0.9	
$\Delta[\frac{\text{Fe}}{\text{H}}]_i = 0.004$	0.2	0.01	0.01	0.1	

8.3.1. p -mode oscillations

The frequencies of p -modes of given degree ℓ are almost quasi-equidistant. Figure 2 represents the variation of $\Delta\nu_{n,\ell} = \nu_{n,\ell} - \nu_{n-1,\ell}$ as a function of the frequency for models A_{BV} and B_{BV} ; n is the radial order of the mode. $\Delta\nu_{n,\ell}$ represents the large spacing between the mode frequencies. It is roughly constant at large frequencies, larger than $2300 \mu\text{Hz}$ for α Cen A and $3500 \mu\text{Hz}$ for α Cen B. Below these frequencies it varies within 10%. In the lower frequency range, $\Delta\nu_{n,\ell}$ has an oscillatory behavior which is the signature of the helium ionization zone (e.g. Gough 1991). We note that it is important to take

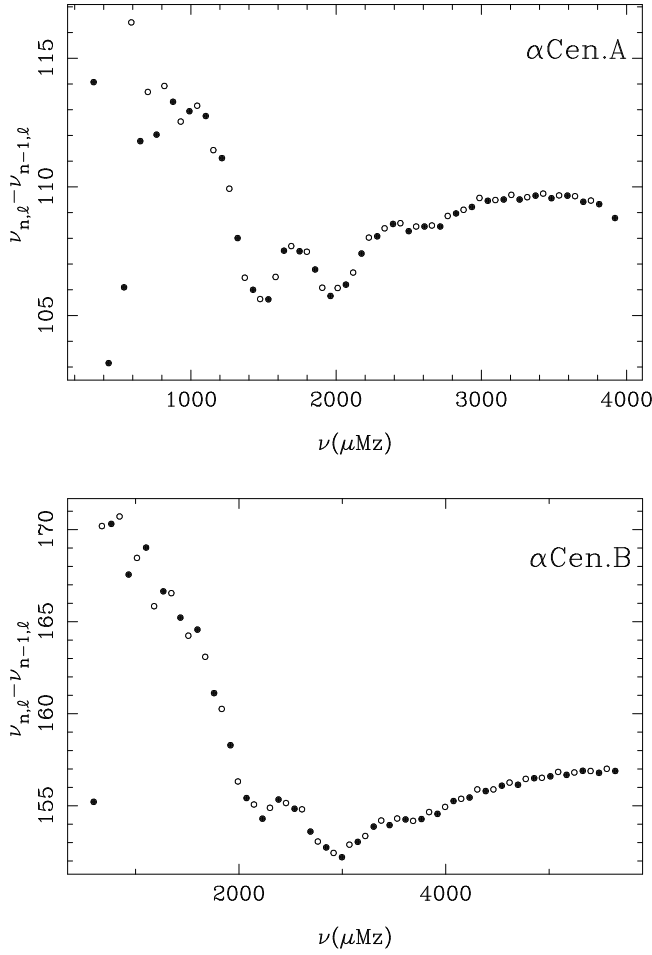


Fig. 2. Variations of the large frequency separations between modes of consecutive radial order $\Delta\nu_{n,\ell} = \nu_{n,\ell} - \nu_{n-1,\ell}$ for p -modes of degree $\ell = 0$ (full point) and $\ell = 1$ (open point) as a function of the frequency for α Cen A & B (models A_{BV} & B_{BV}). The relation between the frequencies and the radial order are taken from Table 8. As asymptotically predicted, $\Delta\nu_{n,\ell}$ is almost constant at high frequency.

into account such a variation while searching peak equidistancy in the p -mode power spectrum.

Another characteristic quantity of the oscillation spectrum is the small separation, i.e. the difference between the frequencies of modes with a degree of same parity and with consecutive radial order:

$$\delta\nu_{\ell,\ell+2} = \nu_{n+1,\ell} - \nu_{n,\ell+2}.$$

This small quantity is very sensitive to the structure of the core mainly to its hydrogen content. Asymptotic analysis predicts that it is proportional to $\ell(\ell+1)$. Figure 3 gives $\delta\nu_{0,2}$ and $\frac{3}{5}\delta\nu_{1,3}$ as a function of the frequencies for the models A_{BV} and B_{BV} . For a given model, these two quantities are very close at high frequencies, as expected from asymptotic approximation and they vary almost linearly

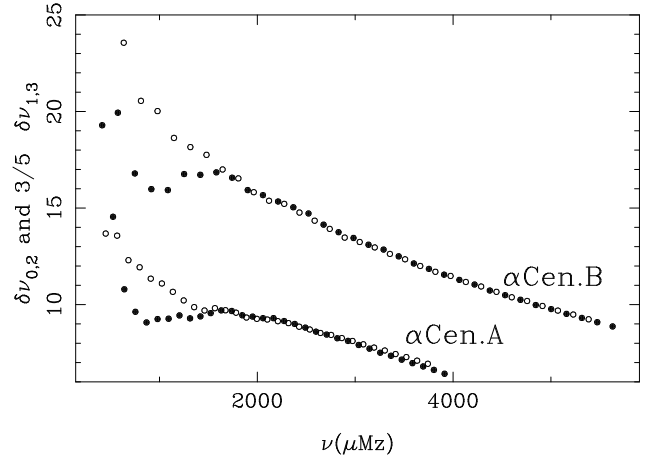


Fig. 3. Variations of the small frequency differences $\delta\nu_{0,2}$ and $\frac{3}{5}\delta\nu_{1,3}$ as a function of the frequency for α Cen A & B (models A_{BV} & B_{BV}). Same symbols as in Fig. 2.

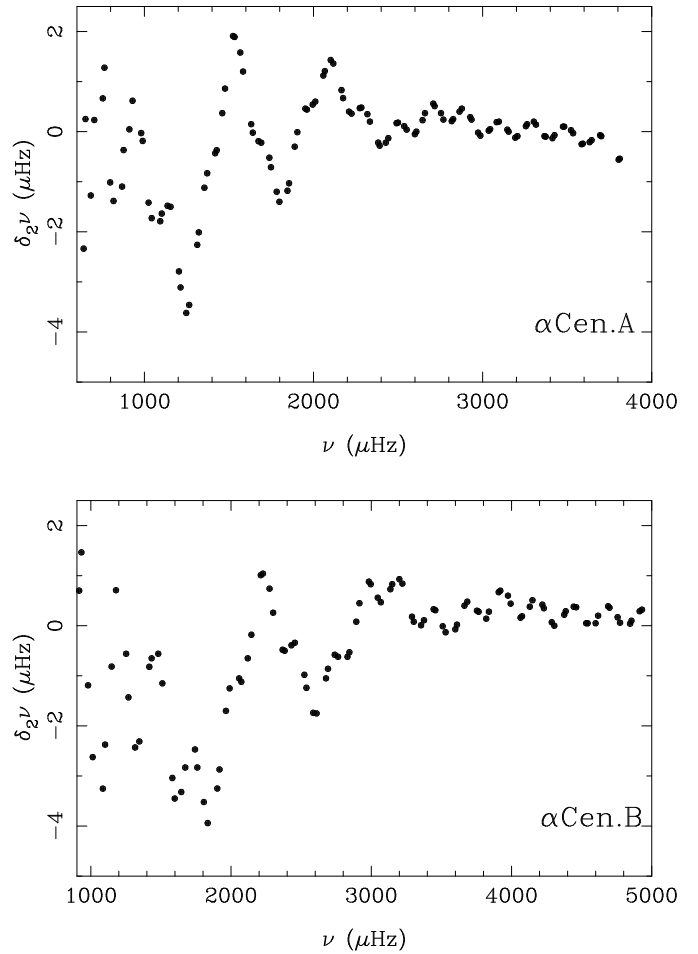


Fig. 4. Variations of the differences of frequencies $\Delta_{n,\ell} = \nu_{n,\ell} - 2\nu_{n+1,\ell} + \nu_{n+2,\ell}$ for p -modes of degree $\ell = 0, 1, 2, 3$ as a function of the frequency for α Cen A & B (models A_{BV} & B_{BV}). The “period” \mathcal{P} of the small oscillation is $203 \mu\text{Hz}$ for A_{BV} and $255 \mu\text{Hz}$ for B_{BV}

with frequency for radial orders n larger than about 16 for α Cen A and 10 for α Cen B.

In the high frequency range the large and small frequency spacings which characterize the p -mode spectrum are usually estimated by analytical fits of the frequencies and of the small frequency separations. The numerical frequencies are fitted by the following polynomial expression (Berthomieu et al. 1993b):

$$\nu_{n,\ell} = \nu_{0\ell} + \Delta\nu_{\ell}(n + \frac{\ell}{2} - n_0) + a_{\ell}(n + \frac{\ell}{2} - n_0)^2.$$

The quantity $\delta\nu_{\ell,\ell+2}$ varies almost linearly with the frequency or the radial order. The small spacing is estimated by using the fit:

$$\delta\nu_{\ell,\ell+2} \sim \overline{\delta\nu}_{\ell,\ell+2} + S_{\ell}(n - n_0).$$

As in the solar case, we consider a set of 9 modes centered at $n_0 \sim 21$, which corresponds approximately to the middle of the range of the expected excited frequencies (i.e. 1 – 3 mHz) for α Cen A, according to Houdek (1996). The fitted coefficients a_{ℓ} are very small. The quantity $\Delta\nu_{\ell}$ does not much depend on the degree, so that $\Delta\nu_{\ell} \sim \Delta\nu_0$ and it characterizes the large frequency spacing. The small spacings are conventionally measured by $\overline{\delta\nu}_{\ell,\ell+2}$. Table 7 shows the quantities ν_{00} , $\Delta\nu_0$, $\overline{\delta\nu}_{0,2}$ and $\overline{\delta\nu}_{1,3}$ which have been computed for the models of α Cen A & B given in Table 5.

These large and small separations of frequency, which characterize the p -mode oscillation spectrum, depend on the stellar mass and age and slightly decrease with the age (Christensen-Dalsgaard 1984, Audard et al. 1995). ν_{00} and $\Delta\nu_0$ are mainly related to the envelope structure of the stellar model and they vary proportionally to $M^{\frac{1}{2}}R^{-\frac{3}{2}}$, while the values of $\overline{\delta\nu}_{0,2}$ and $\overline{\delta\nu}_{1,3}$ reflect the structure in the core.

The computed values of $\Delta\nu_0$ are respectively smaller (*respt.* larger) than the solar ones due to larger (*respt.* smaller) masses of α Cen A (*respt.* α Cen B). These values do not depend much on the description of the convection or on the convective core overshoot, as can be seen from a comparison of the models A_{BV} , A_{CM} , A_{ov} and B_{BV} , B_{CM} , B_{ov} . On the contrary, the value of $\Delta\nu_0$ obtained for the oldest model A_{GD} of α Cen A, which has also a larger mass, is significantly smaller by about 5 μHz . The result is opposite for α Cen B. All these differences can be accounted for by the differences in mass and radius.

The small separations $\overline{\delta\nu}_{0,2}$ and $\overline{\delta\nu}_{1,3}$ decrease with stellar age and mass (Christensen-Dalsgaard 1984). The values of $\overline{\delta\nu}_{0,2}$ and $\overline{\delta\nu}_{1,3}$ obtained for our calibrated models are comparable to those of Pourbaix et al. (1999). As expected, they decrease with the age for the models without core overshoot, and thus are significantly smaller for the A_{GD} model of α Cen A. Future asteroseismic observations could help to discriminate between such models.

The lower panel of Table 7 presents the variations $\Delta[\Delta\nu_0]$, $\Delta[\overline{\delta\nu}_{0,2}]$ and $\Delta[\overline{\delta\nu}_{1,3}]$ for the models computed

with the MLT_{BV} theory and extreme modeling parameters α , $t_{\alpha\text{Cen}}$, Y_i and $[\frac{\text{Fe}}{\text{H}}]_i$ within the confidence domains presented in Table 1. The variations of $\Delta\nu_0$ with α , $t_{\alpha\text{Cen}}$ and Y_i are essentially due to the difference of model radii. The small spacings $\overline{\delta\nu}_{0,2}$ and $\overline{\delta\nu}_{1,3}$ depend mainly on the age and are less sensitive to the differences in radius.

According to Gough (1991), further information on the stellar structure can be provided by low degree oscillations, from the second order difference of frequencies:

$$\Delta_{n,\ell} = \nu_{n,\ell} - 2\nu_{n+1,\ell} + \nu_{n+2,\ell}.$$

When plotted as a function of the frequency (Figure 4), this quantity has a sinusoidal behavior with two different “periods” of order 210 μHz and 700 μHz . The larger period has the largest amplitude and is due to the rapid variation of the adiabatic index Γ_1 in the HeII ionization zone. Its contribution to the frequency is also clearly visible in Fig. 2. The lower period \mathcal{P} is an indication of a discontinuity in the derivative of the sound velocity at the base of the convection zone and is the inverse of twice the travel time of the sound from the surface to the base of the convection zone (e.g. Audard & Provost 1994):

$$\mathcal{P}^{-1} = 2 \int_{R_{\text{cz}}}^{R_{\star}} \frac{dr}{c}.$$

The predicted value of \mathcal{P} is larger for α Cen B than for α Cen A, mainly due to a deeper convection zone for α Cen B (see Table 5). The corresponding amplitude is sensitive to different processes, like convective penetration below the convection zone (e.g. Berthomieu et al. 1993a).

8.3.2. g -mode oscillations

In the low frequency range, the frequencies are mainly determined by the Brunt-Väissälä frequency N . The period of low degree gravity modes is proportional to a characteristic period:

$$\nu_{n,\ell} \sim P_0^{-1}(n + \varepsilon_{\ell}) = \frac{1}{2\pi} \int_{R_{\text{co}}}^{R_{\text{zc}}} \frac{N}{r} dr.$$

The integral, which defines P_0 , is taken in the inner radiative zone, i.e. from the radius of the convective core R_{co} for α Cen A, or from the center for α Cen B, to the base of the external convection zone R_{zc} . For stars without convective core, like the Sun or α Cen B, ε_{ℓ} depends on the degree of the oscillation, $\varepsilon_{\ell} = \ell/2 + \bar{\varepsilon}$; for stars with convective core (like α Cen A) $\varepsilon_{\ell} = \bar{\varepsilon}$ (Christensen-Dalsgaard 1984). Table 7 gives the values of P_0 for the models of α Cen A & B. When the calibration of α Cen A is made with a core overshoot (which increases the extent of the convective core) P_0 is significantly larger (by 23%). The other differences between the values of P_0 for the models of α Cen A & B are accounted for by the differences in mass and in radius.

9. Discussion and conclusion

Detailed evolutionary calculations of the visual binary α Centauri, including the pre main-sequence have been performed using the recent mass determinations of Pourbaix et al. (1999). Models have been constructed using the CEFF equation of state, OPAL opacities, NACRE thermonuclear reaction rates and microscopic diffusion. We have revisited the effective temperatures, surface gravities and metallicities, using published spectroscopic data and taken these quantities as observational constraints. We have determined the most reliable solution within the confidence domains of the observable constraints via a χ^2 minimization. Each solution is characterized by $\varphi = \{t_{\alpha \text{ Cen}}, Y_i, [\frac{\text{Fe}}{\text{H}}]_i, \alpha_A, \alpha_B\}$, where $t_{\alpha \text{ Cen}}$ is the age of the system, Y_i the initial helium content, $[\frac{\text{Fe}}{\text{H}}]_i$ the initial metallicity and α_A and α_B the convection parameters of each star model. We obtained calibrations using different convection theories and adapted values for the mixing-length parameter of each component.

With the basic Böhm-Vitense (1958) mixing-length theory of convection, we derived $\varphi_{\text{BV}} = \{2710 \text{ Myr}, 0.284, 0.257, 1.53, 1.57\}$. With a convective core overshoot of $0.20 H_p$, we obtained $\varphi_{\text{ov}} = \{3530 \text{ Myr}, 0.279, 0.264, 1.64, 1.66\}$. With the Canuto & Mazitelli (1991, 1992) convection theory, we get $\varphi_{\text{CM}} = \{4086 \text{ Myr}, 0.271, 0.264, 0.964, 0.986\}$. Using the mass values and the observational constraints of the “best” model of Guenther & Demarque (2000), with the basic mixing-length theory, we obtained $\varphi_{\text{GD}} = \{5638 \text{ Myr}, 0.300, 0.296, 1.86, 1.97\}$.

We have also performed χ^2 minimizations forcing the use of a unique value for the convection parameters of models of α Cen A & B. We have not reported the results as they are not significantly different from the former ones.

The most striking fact in our results is the small values obtained for the ages which are noticeably smaller than previous studies, except those of Boesgaard & Hagen (1974) and Pourbaix et al. (1999). With respect to the recent models of Guenther & Demarque (2000) this is due mainly to the mass discrepancies resulting from the small differences in distances. The $\sim 5.5\%$ increase between the masses of Pourbaix et al. (1999) we used and those used by Guenther & Demarque (2000) results from by the 1.5% disparity between the revised Hipparcos parallax (Söderhjelm 2000) used by Guenther & Demarque and the orbital parallax determination of Pourbaix et al. As revealed by the χ^2 minimization, in the case of the present calibration of α Cen, the determination of the age appears to be more sensitive to the mass differences than to the basic observational atmospheric constraints namely, effective temperature, gravity – or luminosity – and metallicity. According to our results, no really satisfactory criterion allows to discriminate among different sets of modeling parameters: they all generate models which fit the observational constraints based on H-R diagram analysis

and metallicities. A naive argument, however, can plead in favor of a subsolar age: as the α Cen binary system is formed of metal enriched material, it formed from more processed interstellar matter than the Sun; this may indicate that α Cen is younger than the solar system.

For the models computed with the basic MLT_{BV} theory and fitted on our observational constraints, the mixing-length parameters are noticeably smaller than the convection parameter α_{\odot} of the solar model calibrated with the same physics; the differences are larger than expected from the Ludwig et al. (1999) simulations. For the models fitted to the observational constraints of the “best” model of Guenther & Demarque (2000), the values derived for α bracket the calibrated solar value. For all models computed with MLT_{BV} theory we note that the smaller the age, the smaller the mixing-length parameters.

For models computed with MLT_{CM} convection theory, in accordance with Canuto & Mazitelli (1991, 1992) we obtain mixing length parameters both close to unity and to the convection parameter α_{\odot} of the solar model calibrated with the same physics, $\alpha_A \simeq \alpha_B \simeq \alpha_{\odot} \simeq 1$. This indicates that the convection theory of Canuto & Mazitelli may support the assumption of a universal convection parameter and it seems to provide better fits to observations, as already pointed out by helioseismology as aforesaid in Sect. 3.

For the α Cen A models fitted on our observational constraints, as in the solar model, microscopic diffusion alone is not efficient enough to account for the observed surface lithium depletion. This may indicate that an unknown physical process, at work beneath the outer convection zone, reinforces the microscopic diffusion and gravitational settling to transport the material down to the lithium burning zone. For α Cen B, the only available observation of the surface lithium abundance is an upper limit (Chmielewski et al. 1992): all α Cen B models predict values compatible with this observation except model B_{BV} . The surface lithium depletion of models calibrated with the Guenther & Demarque (2000) observational constraints are close to the observations and, in that sense, they appear to be more satisfactory than models fitted on our observational constraints: in these models there is no need for additional physical process to transport the lithium to its burning zone. But this imply that the small lithium depletion found in the standard solar model and the too large efficiency of the microscopic diffusion in more massive stars result from physical processes which are not active in α Cen, though masses and rotation status are close to solar ones.

All our models with large masses have initial helium contents close to the solar value $Y_{\odot} - 0.003 \leq Y_i \leq Y_{\odot} + 0.010$, while the models with low masses have a high initial helium content $Y_i = Y_{\odot} + 0.026$. With a primordial helium abundance of $Y_0 \approx 0.235$ we get a galactic enrichment of $\frac{\Delta Y}{\Delta Z} \approx 2.0$, both for the Sun and low mass models and

$\frac{\Delta Y}{\Delta Z} = 1.2 - 1.6$ for high mass models. The differences in $\frac{\Delta Y}{\Delta Z}$ between our α Cen models and the Sun are compatible with the scattering found in the solar neighborhood (Pagel & Portinari 1998) and in other binary system calibrations (Fernandes et al. 1998).

We have computed the large and small frequency spacings of acoustic oscillations for all the models. The large separation $\Delta\nu_0$ for the three models with large masses are within $2 \mu\text{Hz}$, despite their differences in age and physics. They are such that $\Delta\nu_0 \sim 107 - 108 \mu\text{Hz}$. The variations of $\Delta\nu_0$ taking into account the uncertainties in the observable constraints, effective temperatures, gravities and metallicities, are of about $\pm 1 \mu\text{Hz}$. For the model A_{GD} of small mass, the large separation, $\Delta\nu_0 \sim 102 \mu\text{Hz}$, is in agreement with the value of Guenther & Demarque (2000) and significantly lower for our other models. The differences in $\Delta\nu_0$ are mainly explained by the differences in mass and radius.

For the three models with large masses the small separations $\overline{\delta\nu}_{0,2}$ vary from 7.5 to $9.1 \mu\text{Hz}$ for α Cen A and are of about $12 \mu\text{Hz}$ for α Cen B. For each model the variations in $\overline{\delta\nu}_{0,2}$ within the observable uncertainties are $\pm 1 \mu\text{Hz}$. For the model A_{GD}, $\overline{\delta\nu}_{0,2}$ is much smaller and in agreement with the value of Guenther & Demarque. All these differences in $\overline{\delta\nu}_{0,2}$ are mainly related to the differences in central hydrogen content, hence in the age.

These results show that the determination of $\Delta\nu_0$ and $\overline{\delta\nu}_{0,2}$ by seismological observations would help to discriminate between the models of α Cen A computed with different masses and to confirm or not the new determination of the masses by Pourbaix et al. This implies an improvement of the accuracy of the observables used to constrain the calibrated models of α Cen A & B. Concerning the comparison with the seismic observations, the large splitting estimated by Pottasch et al. (1992) and Edmonds & Cram (1995) favor Pourbaix et al (1999). masses. The different possible estimations for the large and small spacings $\Delta\nu_0$ and $\overline{\delta\nu}_{0,2}$ by Kjeldsen et al. (1999a) do not allow to discriminate between the models. We note, however, that their estimation $\Delta\nu_0 = 100.8 \mu\text{Hz}$ and $\overline{\delta\nu}_{0,2} = 11.7 \mu\text{Hz}$ is highly improbable.

We conclude that, even for α Cen, the best known binary system, the models are not strongly enough constrained by the available astrometric, photometric and spectroscopic data. In order to deeply test stellar physics additional information on the internal structure is needed. Up to now ground-based observations give tentative evidence for acoustic oscillations in α Cen A. In a few years from now, one can expect that asteroseismology from space e.g. COROT (Baglin et al. 1998), MONS (Kjeldsen et al. 1999b) and MOST (Matthews 1998) missions and from ground, e.g. Concordiaastro (Fossat et al. 2000), will provide data accurate enough to improve our knowledge of stellar interiors.

Acknowledgements. We would like to express our thanks to the referee, Dr. Pourbaix, for helpful advices. This research has made use of the Simbad data base, operated at CDS, Strasbourg, France. This work has been performed using the computing facilities provided by the OCA program “Simulations Interactives et Visualisation en Astronomie et Mécanique (SIVAM)”.

References

- Abbett W.P., Beaver M., Davids B., et al., 1997, ApJ 480, 395
 Abia C., Rebolo R., Beckman J.E., Crivellari L., 1988, A&A 206, 100
 Adelberger E. G., Austin S. M., Bahcall J.N., et al., 1998, Rev. Mod. Phys. 70, 4, 1265
 Alexander D.R., Fergusson J.W., 1994, ApJ 437, 879
 Alonso A., Arribas S., Martínez-Roger C., 1995, A&A 297, 197
 Alonso A., Arribas S., Martínez-Roger C., 1996, A&A 313, 873
 Andersen J., 1991, AAR 3, 91
 Angulo C., Arnould M., Rayet M., and the NACRE collaboration, 1999, Nuclear Physics A 656, 1, and WEB site <http://pntpm.ulb.ac.be/Nacre/nacre.htm>
 Audard N., Provost J., 1994, A&A 282, 73
 Audard N., Provost J., Christensen-Dalsgaard J., 1995, A&A 297, 427
 Baglin A., and the COROT team, 1998, Asteroseismology from space – The COROT mission. In: F.L. Deubner, J. Christensen-Dalsgaard & D. Kutz (eds.) New Eyes to See Inside the Sun and Stars, IAU Symposium 185, 301
 Bell R.A., Ericksson K., Gustafsson B., Nordlund A., 1976, A&AS 23, 37
 Berthomieu G., Morel P., Provost J., Zahn J.P., 1993a, Seismological constraints on the convective penetration in the Sun. In: Baglin A. & Weiss W.W. (eds.) Inside the Stars, IAU Colloquium 137, ASP Conf. Series 40, 60
 Berthomieu G., Provost J., Morel P., Lebreton Y., 1993b, A&A 262, 775
 Bessell M.S, 1981, Proc. Astron. Soc. Australia 4, 212
 Boesgaard A.M., Hagen W., 1974, ApJ 189, 85
 Böhm-Vitense E., 1958, Z. Astrophys. 54, 114
 Brown T.M., Gilliland R.L., 1990, ApJ 350, 839
 Brown T.M., Christensen-Dalsgaard J., Weibel-Mihalas B., Gilliland R.L., 1994, ApJ 427, 1013
 Canuto V.M., Mazitelli I., 1991, ApJ 370, 295
 Canuto V.M., Mazitelli I., 1992, ApJ 389, 729
 Cayrel R., 2000, private communication
 Chmielewski Y., Friel E., Cayrel de Strobel G., Bentolila C., 1992, A&A 263, 219
 Christensen-Dalsgaard J., 1984, What will asteroseismology teach us?. In: Mangeney A. & Praderie F. (eds.) Space Research Prospects in Stellar Activity and Variability, Pub. Obs. Paris-Meudon 11, 11
 Christensen-Dalsgaard J., Berthomieu G., 1991, Solar interior and atmosphere. In: Cox A.N., Livingston W.C. & Matthews M.S. (eds.), The University of Arizona Press, Tucson, 401
 Christensen-Dalsgaard J., Däppen W., 1992, A&A Rev. 4, 267
 Christensen-Dalsgaard J., Däppen W., Antia H.M., et al., 1996, Science 272, 1286
 Clayton D.D., 1968, Principles of Stellar Evolution and Nucleosynthesis, Mc Graw-Hill

- Couteau P., 1978, *L'Observation des Etoiles doubles Visuelles*, Flammarion
- Demarque P., Guenter D.B., van Altena W.F., 1986, *ApJ* 300, 773
- Edmonds P., Cram L., Demarque P., et al., 1992, *ApJ* 394, 313
- Edmonds P., Cram L., 1995, *MNRAS* 276, 1295
- ESA, 1997, *The Hipparcos and Tycho Catalogues*. ESA SP-1200
- England M.N., 1980, *MNRAS* 191, 23
- Edvardsson B., 1988, *A&A* 190, 148
- Edvardsson B., Andersen J., Gustafsson B., et al., *A&A* 275, 101
- Fernandes J., Neuforge C., 1995, *A&A* 295, 678
- Fernandes J., Lebreton Y., Baglin A., Morel P., 1998, *A&A* 338, 455
- Flannery B.P., Ayres T.R., 1978, *ApJ* 221, 175
- Fossat E., Grec G., Vernin J., 2000, private communication and WEB site <http://www-astro.unice.fr/concord/CSA/index.htm>
- French V.A., Powell A.L.T., 1971, *R. Obs. Bull.* 173
- Freytag B., Ludwig H.G., Steffen M., 1999, A calibration of the mixing-length for solar-type stars based on hydrodynamical simulations of the surface layers. In: Giménez A., Guinan E.F. & Montesinos B. (eds.) *Theory and Tests of Convection in Stellar Structure*. ASP, Conf. Series, 173, 225
- Furenlid I., Meylan T., 1990, *ApJ* 350, 827
- Gelly B., Grec G., Fossat E., 1986, *A&A* 164, 383
- Gough D.O., 1991, Comments on Helioseismic Inference. In: Osaki Y. & Shibahashi H. (eds.) *Progress of Seismology of the Sun and Stars*, Springer Verlag, 283
- Grevesse N., Noels A., 1993, Cosmic Abundances of the Elements. In: Prantzos N., Vangioni-Flam E. & Casse M. (eds.) *Origin and Evolution of the Elements*. Cambridge University Press, 14
- Grevesse N., Sauval A.J., 1998, Standard Solar Composition. In: Frölich C., Huber M.C.E., Solanki S.K. & Von Steiger R. (eds.) *Solar Composition and its Evolution - from Core to Corona*, ISSI workshop, Space Sciences Series of ISSI 5, 161
- Guenter D.B., Demarque P., 2000, *ApJ* 531, 503
- Heintz W., 1958, *Veröff. Münch* 5, 100
- Heintz W., 1982, *Observatory* 102, 42
- Houdek G., 1996, Ph.D. Thesis, "Pulsation of Solar-type stars", Formal und Naturwissenschaftliche Fakultät der Universität Wien
- Houdek G., Balmforth N.J., Christensen-Dalsgaard J., Gough D., 1999, *A&A* 351, 582
- Iglesias C.A., Rogers F.J., Wilson B.G., 1992, *ApJ* 397, 717
- Iglesias C.A., Rogers F.J., 1996, *ApJ* 464, 943
- Kamper K.W., Wesselink A.J., 1978, *AJ* 83, 1653
- King R.J., Deliyannis C.P., Hiltgen D.D., et al., 1997, *AJ* 113, 1871
- Kjeldsen H., Bedding T.R., Frandsen S., Dall T.H., 1999a, *MNRAS* 303, 579
- Kjeldsen H., Bedding T.R., Christensen-Dalsgaard J., 1999b. MONS, Measuring Oscillations in Nearby Stars, A proposal for the Danish Satellite Programme, Document N0 MONS-99/01
- Kurucz R.L., 1991, Stellar Atmospheres: Beyond Classical Models. In: Crivellari L., Hibeny I. & Hammer D.G. (eds.), NATO ASI Series, Kluwer, Dordrecht
- Lastennet E., Valls-Gabaud D., Lejeune Th., Oblack E., 1999, *A&A* 349, 494
- Lebreton Y., Perrin M.-N., Cayrel R., et al., 1999, *A&A* 350, 587
- Lejeune Th., Cuisinier F., Buser R., 1998, *A&AS* 130, 65
- Ludwig H.G., Freytag B., Steffen M., 1999, *A&A* 346, 111
- Lydon T.J., Fox P.A., Sofia S., 1993, *ApJ* 413, 390L
- Mathews J.M., 1998, Asteroseismology from space: Getting the MOST science for the least money. In: Korzennik S. & Wilson A. (eds), SOHO6/GONG98. Structure and Dynamics of the Interior of the Sun and Sun-like Stars, ESA Publication SP-418, 395
- Mermillod J.C., Mermillod M., Hauck B., 1997, *A&AS* 124, 349
- Michaud G., 1977, *Nat.* 266, 433
- Michaud G., Proffitt C.R., 1993, Particule Transport Process. In: Baglin A. & Weiss W.W. (eds.) *Inside the Stars*, IAU Colloquium 137, ASP Conference Series, 40, 246
- Montalbàn J., Schatzman E., 2000, *A&A* 354, 943
- Morel P., van't Veer C., Provost J., et al., 1994, *A&A* 286, 91
- Morel P., 1997, *A&AS* 124, 597
- Morel P., Provost J., Berthomieu G., 1997, *A&A* 327, 349
- Morel P., Provost J., Berthomieu G., 2000a, *A&A* 353, 771
- Morel P., Morel Ch., Provost J., Berthomieu G., 2000b, *A&A* 354, 636
- Noels A., Grevesse N., Magain P., et al., 1991, *A&A* 247, 91
- Neuforge C., 1993, *A&A* 268, 650
- Neuforge-Verheecke C., Magain P., 1997, *A&A* 328, 261
- Pagel B.E.J., Portinari L., 1998, *MNRAS* 298, 747
- Perryman M.A.C., Brown A.G.A., Lebreton Y., et al., 1998, *A&A* 331, 81
- Pottasch E.M., Butcher H.R., van Hoesel F.H.J., 1992, *A&A* 264, 138
- Pourbaix D., Neuforge-Verheecke C., Noels A., 1999, *A&A* 344, 172
- Primas F., Duncan D.K., Pinseanneault M.H., et al., 1997, *ApJ* 480, 784
- Provost J., Berthomieu G., Morel P., 2000, *A&A* 353, 775
- Rabolo R., Crivellari L., Castelli F., et al., 1986, *A&A* 166, 195
- Richer J., Michaud G., Turcotte S., 2000, *ApJ* 529, 338
- Saar S.H., Osten R.A., 1997, *MNRAS* 284, 803
- Salpeter E.E., 1954, *Australian J. Phys.* 7, 373
- Schaller G., Schaerer D., Meynet G., Maeder A., 1992, *A&AS* 96, 269
- Schatzman E., 1996, *J. Fluids Mech.* 322,355
- Smith G., Edvardsson B., Frisk U., 1986, *A&A* 165, 126
- Soderblom D.R., Dravin D., 1984, *A&A* 140, 127
- Söderhjelm S., 2000, *A&A* 341, 121
- Thévenin F., 1998, *Bull. CDS* 49, catalog III/193
- Thomas J.A., Hyland A.R., Robinson G., 1973, *MNRAS* 165, 201
- Turcotte S., Richer J., Michaud G., et al., 1998, *ApJ* 504, 539
- Zahn J.P., 1992, *A&A* 265, 115

Table 5. All symbols have their ordinary meaning. {The brackets indicate values derived from basic formula.}

Top, left panel: adopted observational data to be reached by the calibration.

Top, right panel: Observational constraints of the “best” model of Guenther & Demarque (2000).

Bottom panel: Characteristics of α Cen A & B and Sun models computed with the same input physics. The α Cen A (*respt.* α Cen B) models are named “A.” (*respt.* “B.”). The first four rows recall some items of Table 1: the ages (Myr), the initial helium mass fractions, the initial heavy element to hydrogen mass ratios, and the mixing-length parameters. The next three rows give the effective temperatures in K, the surface gravities and the metallicities. The six next rows present respectively the luminosities, the total radii in solar units, the surface mass fractions of hydrogen and helium, the ratios of heavy element to hydrogen and the lithium abundances. In the next rows R_{cz} and T_{cz} are respectively the radius and the temperature (in MK) at the base of the external convection zone, R_{co} is the radius of the convective core (including overshoot for model A_{ov} & B_{ov}). At center, T_c , ρ_c , X_c , Y_c are respectively the temperature (in MK), the density (in g cm^{-3}), the hydrogen and the helium mass fractions.

	Models BV, _{ov} & CM				Models GD			
	α Cen A		α Cen B		α Cen A		α Cen B	
M/M_\odot	1.16 ± 0.031		0.97 ± 0.032		1.1015 ± 0.008		0.9159 ± 0.007	
T_{eff}	5790 ± 30 K		5260 ± 50 K		5770 ± 50 K		5300 ± 50 K	
$\log g$	4.32 ± 0.05		4.51 ± 0.08		$\{4.28 \pm 0.02$		$4.54 \pm 0.03\}$	
$[\frac{\text{Fe}}{\text{H}}]$	0.20 ± 0.02		0.23 ± 0.03		0.22 ± 0.02		0.26 ± 0.04	
L/L_\odot	$\{1.534 \pm 0.103$		$0.564 \pm 0.064\}$		1.572 ± 0.135		0.509 ± 0.06	

	Models with MLT _{BV} theory						Models with MLT _{CM} theory			
	A _{BV}	B _{BV}	A _{ov}	B _{ov}	A _{GD}	B _{GD}	\odot_{BV}	A _{CM}	B _{CM}	\odot_{CM}
$t_{\alpha \text{ Cen}}$	2710		3530		5640		4685	4086		4685
Y_i	0.284		0.279		0.300		0.274	0.271		0.274
$(\frac{Z}{X})_i$	0.0443		0.0450		0.0480		0.0279	0.0450		0.0279
α	1.53	1.57	1.64	1.66	1.86	1.97	1.93	0.96	0.99	1.03
T_{eff}	5795	5269	5795	5269	5759	5332	5778	5794	5268	5778
$\log g$	4.324	4.508	4.316	4.509	4.286	4.523	4.438	4.324	4.522	4.438
$[\frac{\text{Fe}}{\text{H}}]$	0.20	0.23	0.20	0.23	0.22	0.25	0.000	0.20	0.23	0.000
L/L_\odot	1.527	0.571	1.555	0.569	1.565	0.547	1.000	1.526	0.552	1.000
R/R_\odot	1.228	0.909	1.239	0.907	1.259	0.867	1.000	1.228	0.893	1.000
X_s	0.722	0.701	0.729	0.708	0.711	0.695	0.737	0.735	0.717	0.737
Y_s	0.250	0.270	0.243	0.262	0.260	0.275	0.245	0.236	0.253	0.245
$[\text{Li}]_s$	2.72	1.10	2.54	0.496	1.94	-3.32	2.46	2.33	-0.54	2.46
$(\frac{Z}{X})_s$	0.0384	0.0418	0.0385	0.0419	0.0410	0.0433	0.0245	0.0386	0.0418	0.0245
R_{cz}/R_\star	0.776	0.698	0.758	0.692	0.707	0.675	0.715	0.741	0.685	0.715
T_{cz}	1.503	2.585	1.644	2.653	2.020	2.846	2.178	1.801	2.761	2.178
R_{co}/R_\star	0.026		0.054		0.061			0.038		
T_c	17.00	13.66	17.46	13.76	19.43	14.26	15.77	17.74	13.71	15.76
ρ_c	126.0	96.28	125.5	100.8	172.0	123.7	155.9	146.8	102.4	155.9
X_c	0.374	0.540	0.387	0.510	0.178	0.400	0.330	0.283	0.497	0.330
Y_c	0.594	0.428	0.580	0.458	0.788	0.566	0.649	0.684	0.470	0.649

Table 6. Partial derivatives of observables $\log T_{\text{eff A}}$, $\log \frac{L_{\text{A}}}{L_{\odot}}$, $[\frac{\text{Fe}}{\text{H}}]_{\text{A}}$, $\log T_{\text{eff B}}$, α_{B} , $\log \frac{L_{\text{B}}}{L_{\odot}}$ and $[\frac{\text{Fe}}{\text{H}}]_{\text{B}}$ with respect to modeling parameters $t_{\alpha \text{ Cen}}(\text{Myr})$, α_{A} , α_{B} , Y_{i} and $[\frac{\text{Fe}}{\text{H}}]_{\text{i}}$ of models A_{BV} & B_{BV}.

	$\partial \log T_{\text{eff A}}$	$\partial \log \frac{L_{\text{A}}}{L_{\odot}}$	$\partial [\frac{\text{Fe}}{\text{H}}]_{\text{A}}$	$\partial \log T_{\text{eff B}}$	$\partial \log \frac{L_{\text{B}}}{L_{\odot}}$	$\partial [\frac{\text{Fe}}{\text{H}}]_{\text{i}}$
$\partial t_{\alpha \text{ Cen}}$	$-2.15 \cdot 10^{-7}$	$4.16 \cdot 10^{-5}$	$-2.30 \cdot 10^{-5}$	$1.63 \cdot 10^{-6}$	$2.32 \cdot 10^{-5}$	$-9.24 \cdot 10^{-6}$
$\partial \alpha_{\text{A}}$	0.0380	$8.23 \cdot 10^{-3}$	0.0541	0.	0.	0.
$\partial \alpha_{\text{B}}$	0.	0.	0.	0.0306	0.0213	$5.67 \cdot 10^{-3}$
∂Y_{i}	0.469	3.85	-0.911	0.621	3.55	-0.185
$\partial [\frac{\text{Fe}}{\text{H}}]_{\text{i}}$	$-2.12 \cdot 10^{-3}$	-0.014	0.024	$-2.40 \cdot 10^{-3}$	-0.0129	0.0205

Table 8. Low degree frequencies for α Cen A and B.

n	α Cen A, model A _{BV}				α Cen B, model B _{BV}			
	$\ell = 0$	$\ell = 1$	$\ell = 2$	$\ell = 3$	$\ell = 0$	$\ell = 1$	$\ell = 2$	$\ell = 3$
1	216.50	239.04	332.72	354.66	280.33	313.25	404.94	460.11
2	330.58	357.01	414.45	450.61	439.72	504.26	575.00	635.19
3	433.74	473.41	525.29	567.19	594.94	674.45	748.46	810.92
4	539.84	589.81	640.82	683.00	765.25	845.17	916.83	980.26
5	651.62	703.50	754.02	797.53	932.81	1013.63	1085.89	1148.42
6	763.65	817.42	867.89	911.05	1101.83	1179.48	1251.72	1315.75
7	876.96	929.96	980.65	1024.62	1268.49	1346.02	1416.99	1480.67
8	989.90	1043.11	1093.39	1136.78	1433.70	1510.26	1581.42	1645.03
9	1102.65	1154.54	1204.33	1247.43	1598.27	1673.35	1742.83	1806.05
10	1213.79	1264.47	1312.49	1354.49	1759.39	1833.61	1901.74	1963.56
11	1321.79	1370.95	1418.40	1460.41	1917.69	1989.93	2057.43	2119.37
12	1427.80	1476.58	1523.87	1566.71	2073.10	2145.00	2212.06	2274.53
13	1533.43	1583.08	1631.25	1674.60	2227.40	2299.89	2367.70	2430.43
14	1640.95	1690.78	1738.77	1782.29	2382.75	2455.04	2522.86	2585.94
15	1748.45	1798.25	1845.79	1888.78	2537.58	2609.85	2677.04	2739.71
16	1855.24	1904.34	1951.62	1994.97	2691.18	2762.91	2830.18	2892.90
17	1961.01	2010.40	2057.91	2101.70	2843.92	2915.35	2982.68	3046.16
18	2067.20	2117.07	2165.32	2209.86	2996.13	3068.24	3136.07	3200.00
19	2174.62	2225.10	2273.55	2318.42	3149.16	3221.60	3290.20	3354.77
20	2282.71	2333.49	2382.26	2427.33	3303.04	3375.80	3444.50	3509.53
21	2391.27	2442.08	2490.76	2536.02	3456.99	3530.11	3599.13	3664.29
22	2499.56	2550.55	2599.41	2644.81	3611.26	3684.29	3753.67	3819.43
23	2608.02	2659.04	2708.02	2753.86	3765.55	3838.97	3908.55	3974.76
24	2716.48	2767.90	2817.19	2863.25	3920.10	3993.88	4064.07	4130.66
25	2825.46	2877.03	2926.58	2973.04	4075.36	4149.28	4219.77	4286.93
26	2934.69	2986.58	3036.24	3082.83	4230.79	4305.15	4375.88	4443.28
27	3044.15	3096.07	3145.94	3192.80	4386.60	4461.07	4532.20	4600.01
28	3153.68	3205.77	3255.68	3302.66	4542.70	4617.33	4688.59	4756.82
29	3263.18	3315.36	3365.50	3412.70	4698.84	4773.76	4845.36	4913.76
30	3372.84	3425.10	3475.26	3522.63	4855.34	4930.30	5002.17	5070.99
31	3482.42	3534.76	3585.10	3632.58	5011.94	5087.14	5159.10	5228.14
32	3592.07	3644.40	3694.70	3742.31	5168.62	5243.95	5316.22	5385.43
33					5325.52	5400.85	5473.22	5542.77